Letter | Editors' Suggestion

# Hole-$Cr^+$ nanomagnet in a semiconductor quantum dot

V. Tiwari,[1] M. Arino,[2] S. Gupta,[3] M. Morita,[2] T. Inoue,[2] D. Caliste,[3] P. Pochet,[3] H. Boukari,[1] S. Kuroda,[2] and L. Besombes[1,*]

[1]*Institut Néel, CNRS, Univ. Grenoble Alpes and Grenoble INP, 38000 Grenoble, France*
[2]*Institute of Materials Science, University of Tsukuba, Tsukuba 305-8573, Japan*
[3]*Department of Physics, IriG, Univ. Grenoble Alpes and CEA, 38000 Grenoble, France*

(Received 7 May 2021; revised 1 July 2021; accepted 6 July 2021; published 23 July 2021)

We study a diluted magnetic semiconductor system based on the spin of the ionized acceptor $Cr^+$. We show that the negatively charged $Cr^+$ ion, an excited state of the Cr in II-VI semiconductor, can be stable when inserted in a CdTe quantum dot (QD). The $Cr^+$ attracts a heavy hole in the QD and form a stable hole-$Cr^+$ complex. Optical probing of this system reveals a ferromagnetic coupling between heavy holes and $Cr^+$ spins. At low temperature, the thermalization on the ground state of the hole-$Cr^+$ system with parallel spins prevents the optical recombination of the excess electron on the $3d$ shell of the atom. We study the dynamics of the nanomagnet formed by the hole-$Cr^+$ exchange interaction. The ferromagnetic ground states with $M_z = \pm 4$ can be controlled by resonant optical pumping and a spin relaxation time in the 20 $\mu$s range is obtained at $T = 4.2$ K. This spin memory at zero magnetic field is limited by the interaction with phonons.

DOI: 10.1103/PhysRevB.104.L041301

Recent experimental breakthroughs have laid the foundations for atomic scale data storage, showing the capability to read and control the spin of a single magnetic atom. In particular, a magnetic atom can develop a magnetic anisotropy energy when it interacts with the surface of a metal and behaves like a nanomagnet [1]. A single magnetic atom can also present a large magnetic anisotropy and a spin memory when interacting with ligands in a molecular magnet [2]. In semiconductors, the optical properties of a quantum dot (QD) can be used to control the spin of individual magnetic atoms [3–10]. Embedding a magnetic atom in a QD offers in addition the possibility to tune the environment of the localized spin. A control of the charge of the QD can for instance influence the magnetic anisotropy of the atom [11], making these nanosized systems attractive for miniaturized data storage applications.

A variety of magnetic transitions metals can be incorporated in semiconductors offering a large choice of localized electronic spins, nuclear spins as well as orbital momentum. The $3d^5$ $Mn^{2+}$, a pure spin without orbital momentum, is the most widely studied magnetic element in nanostructures [12,13]. The magnetic properties of these nanostructures are mainly controlled by the exchange interaction of the holes spins with the five $d$ electrons of the atom. In a II-VI compound, this exchange interaction is dominated by $p-d$ hybridization, the so-called kinetic exchange with antiferromagnetic sign [14–17]. This antiferromagnetic interaction limits the spin stability of the complex formed by a heavy hole and one or a few Mn atoms as hole-Mn spins flip-flops occur in the magnetic ground state [11].

We demonstrate here that another $3d^5$ element, the negatively charged ionized acceptor $Cr^+$, can be optically probed when inserted in CdTe/ZnTe QDs. We study the spin properties of this diluted magnetic semiconductor system. The negative charge of the $Cr^+$ ion attracts a hole in the QD and the hole-$Cr^+$ complex is formed. Magneto-optics measurements on these positively charged QDs show that the hole-$Cr^+$ exchange interaction is ferromagnetic. This coupling leads to a ground state configuration with parallel hole and $Cr^+$ spins which blocks the recombination of the excess electron of the $3d$ shell. The two low energy hole-$Cr^+$ states, with angular momentum $M_z = \pm 4$, behave like an Ising spin system that can thus be seen as a nanomagnet. Resonant optical pumping is used to probe the dynamics of the hole-$Cr^+$ complex. A spin memory in the 20 $\mu s$ range is observed at $T = 4.2$ K and zero magnetic field. This dynamics is controlled by the interaction with phonons.

For these experiments, Cr atoms are randomly introduced in CdTe/ZnTe QDs grown by molecular beam epitaxy on a 1 $\mu$m thick ZnTe buffer layer deposited on a GaAs (001) substrate [18]. The amount of Cr is adjusted to obtain QDs containing 0, 1, or a few Cr atoms. Individual QDs are studied in magnetic field by optical microspectroscopy [19].

A free Cr atom exhibits a $3d^5 4s^1$ electron configuration. In the cation site of a II-VI semiconductor, two of its electrons are given to the bonds. The isoelectronic impurity $Cr^{2+}$ ($3d^4$) is formed with a spin $S = 2$ and an orbital momentum $L = 2$. However, in CdTe, $Cr^{2+}$ is also an acceptor [23–25]. This is illustrated in Fig. 1 presenting density functional theory based calculations of substitutional Cr in CdTe (DFT code BigDFT [19,26–28]). A Cr sitting on a Cd site is adopting a 2+ oxidation state with two occupied levels in the valence band, two occupied and one unoccupied levels below the conduction band edge [Fig. 1(a)]. The Cr can then capture an electron on its unoccupied level; it adopts a 1+ oxidation state ($3d^5$, $S = 5/2$ and $L = 0$) with five localized levels in the band gap,

*lucien.besombes@neel.cnrs.fr

 

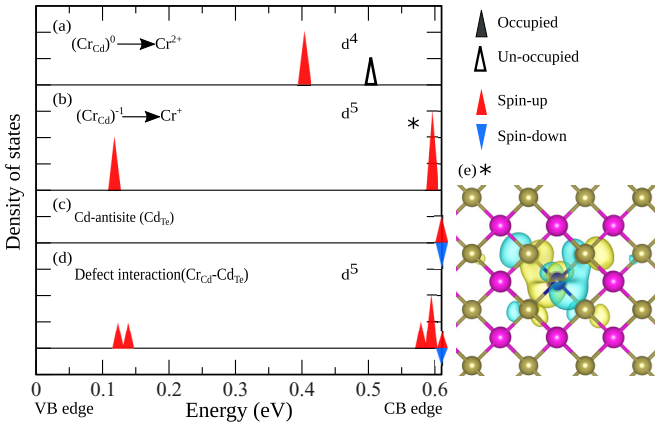


FIG. 1. DFT calculated defects electronic levels in the band gap of CdTe for a $Cr^{2+}$ (a), a $Cr^{+}$ (b) along with (c) a Cd antisite compared to a configuration (d) where the $Cr_{Cd}$ and $Cd_{Te}$ are separated by 9.5 Å. (e) Calculated orbital of one of the states in the high energy triplet of the $Cr^{+}$ showing the hybridization of Cr and Te orbitals.

a low energy doublet, and a high energy triplet [Fig. 1(b)]. The triplets states are significantly mixed with the anion $p$ orbitals [Fig. 1(e)]. This $p-d$ hybridization is a potential source of kinetic exchange between the $Cr^{+}$ and holes spins [14–17].

The negatively charged acceptor $Cr^{+}$ is however unstable in bulk II-VI materials. Its magnetic properties and exchange interaction with the carriers of the host have never been studied. The presence of $Cr^{+}$ was nevertheless detected in electron paramagnetic resonance experiments in bulk n-type CdTe or under optical excitation [23,24].

We used DFT calculations to evaluate the influence of defects on the possibility to observe $Cr^{+}$ in undoped CdTe. Indeed, charge compensation with intrinsic point defects is a common mechanism [29]. We found that a Cd antisite (donor character) can give rise to a change in the oxidation state of the Cr. Figure 1 depicts the defects states for isolated Cr and Cd antisite as compared to a configuration where they are located at a distance of 9.5 Å (third neighbor). The latter configuration presents five states in the band gap with five unpaired electrons [Fig. 1(d)]. Even at this small distance, the electronic states are located on the Cr center with energies and orbitals very similar to a $3d^5$ isolated $Cr^{+}$. Similarly, Zn antisite in the barriers of Cr-doped CdTe/ZnTe QDs could be a local source of electron transfer to $Cr^{2+}$ by modulation doping.

QDs containing an individual isoelectronic $Cr^{2+}$ were identified recently [30]. In these dots, the spin $S=2$ of $Cr^{2+}$ is split by a large fine structure term induced by local strain. At low temperature, the exchange interaction with a confined exciton gives rise to three main emission lines corresponding to the lowest energy spin states of the atom $S_z=0$ and $S_z=\pm 1$.

Figure 2 presents the magnetic field dependence of another type of QDs observed in Cr-doped samples. Their emission consists in a minimum of six lines equally spaced in energy (see QD1) [31]. Most of these QDs present a more complex structure with the third line clearly split and seven lines separated by a gap (see QD2). The width of the gap changes from dot to dot and additional weak intensity lines can also be observed [19]. No linear polarization was observed in any of the investigated QDs [Fig. 2(c)] suggesting that this PL

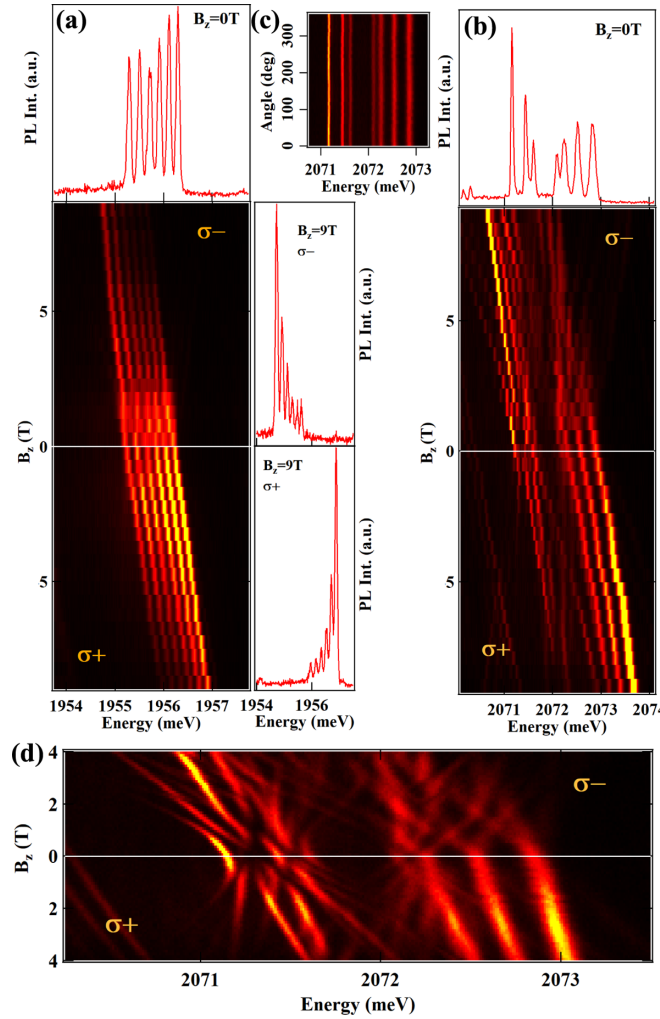


FIG. 2. Magnetic field dependence of the PL of two positively charged QDs, QD1 (a) and QD2 (b) containing a $Cr^{+}$. The bottom panels present PL intensity maps recorded in circular polarization. (c) Linear polarization PL intensity map of QD2 at $B_z=0$ T. (d) Detail of the PL intensity map of QD2.

structure arises from a charged exciton (i.e., absence of fine structure splitting) [32].

Under magnetic field each line presents a Zeeman splitting and a change in the photoluminescence (PL) intensity distribution is observed. At $B_z=9$ T the PL is concentrated on the low energy lines in $\sigma-$ polarization and on the high energy lines in $\sigma+$ polarization [Fig. 2(a)]. This intensity distribution is influenced by the temperature and the excitation power and is opposite the situation reported for $Mn^{2+}$ in II-VI QDs [3,19]. A line broadening or anticrossings are usually observed in the low magnetic field region. This is particularly pronounced for QD2 where a complex series of anticrossings is observed below $B_z=4$ T [Fig. 2(d)].

This PL structure can be explained by the recombination of a positively charged exciton ($X^{+}$) interacting with the spin $S=5/2$ of the Cr in its $3d^5$ configuration, the $Cr^{+}$ ionized acceptor. This charged ion, when located in a QD, attracts a hole and repels electrons. Thus, a hole-$Cr^{+}$ complex is formed that can be probed by the optical injection of an exciton.

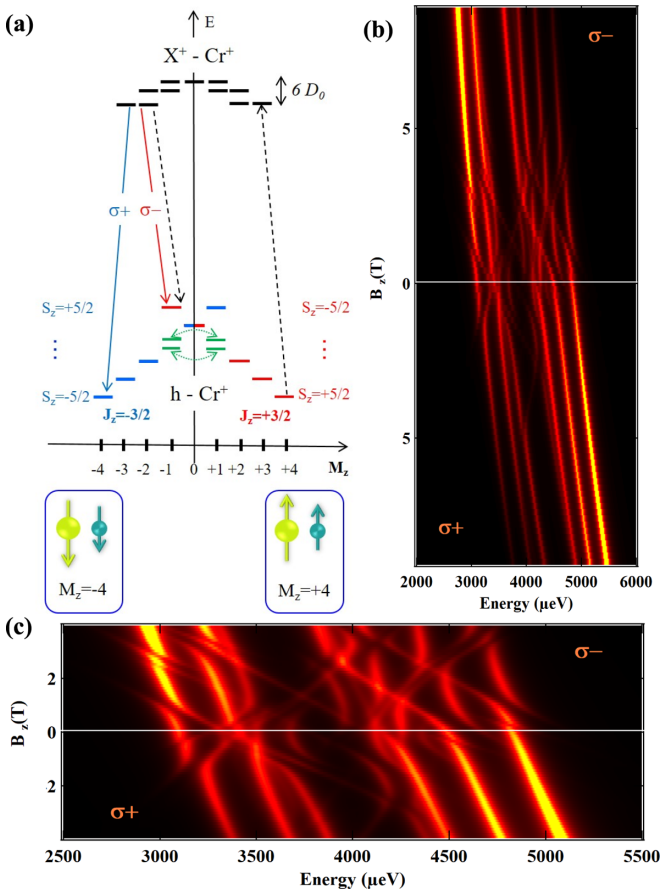


FIG. 3. (a) Energy levels of the excited state (X$^+$-Cr$^+$) and ground state ($h$-Cr$^+$) in a positively charged Cr$^+$-doped QD. The electron-Cr exchange interaction and the fine structure term $E$ are neglected and the structure of X$^+$-Cr$^+$ is controlled by $D_0$. The most intense transitions in $\sigma+$ and $\sigma-$ polarizations are indicated with thick arrows. Dashed arrows show the excitation/detection configuration for the pumping experiment. (b) PL intensity map of $X^+ - Cr^+$ calculated with $I_{eCr^+} = 0$ $\mu$eV, $I_{hCr^+} = -225$ $\mu$eV, $D_0 = -40$ $\mu$eV, $E = 20$ $\mu$eV, $T_{\text{eff}} = 20$ K, $\rho/\Delta_{\text{lh}} = 0.2$, $\theta_s = -\pi/4$ and $\gamma = 1.5$ $\mu$eV T$^{-2}$, $g_{Cr^+} = 2$, $g_h = 0.5$, $g_e = -0.4$. (c) Detail of the calculated PL intensity map.

This attribution is confirmed by the modeling of the magnetic field dependence of X$^+$-Cr$^+$ presented in Fig. 3. In this model, we consider that the two holes are not localized on the negatively charged acceptor and keep a heavy-hole character with a spin $J_z = \pm 3/2$ [33]. The energy levels of X$^+$-Cr$^+$ are then described by the Hamiltonian

$$\mathcal{H}_{X^+-Cr^+} = I_{eCr^+}\vec{S}\cdot\vec{\sigma} + g_e\mu_B\vec{\sigma}\cdot\vec{B} + \gamma B^2 + \mathcal{H}_{Cr^+} \qquad (1)$$

which contains the exchange interaction between the Cr spin ($\vec{S}$) and the electron spin ($\vec{\sigma}$), the Zeeman energy of the electron spin and a quadratic diamagnetic shift. $\mathcal{H}_{Cr^+} = D_0 S_z^2 + E(S_x^2 - S_y^2) + g_{Cr^+}\mu_B\vec{S}\cdot\vec{B}$ contains the fine structure of the Cr$^+$ spin and its Zeeman energy with $g_{Cr^+} \approx 2$ [24,36]. The strain induced fine structure consists of a biaxial term $D_0$ and a term arising from a possible in-plane anisotropy $E$. The exchange interaction of the two spin paired holes with the Cr$^+$ is neglected [37,38].

For $I_{eCr^+} \gg D_0$ and $E$, $\mathcal{H}_{X^+-Cr^+}$ describes the isotropic coupling of a spin 5/2 and a spin 1/2. This would result in two energy levels with a total angular momentum $M = 2$ or $M = 3$ and split by $3I_{eCr^+}$. For a vanishingly small $I_{eCr^+}$, energies of X$^+$-Cr$^+$ are dominated by the fine structure $\mathcal{H}_{Cr^+}$.

The hole-Cr$^+$ complex in the ground state is described by

$$\mathcal{H}_{h\text{-}Cr^+} = I_{hCr^+}\vec{S}\cdot\vec{J} + g_h\mu_B\vec{J}\cdot\vec{B} + \mathcal{H}_{Cr^+} \qquad (2)$$

where $\vec{J}$ is the hole spin operator. In the subspace of the two low-energy heavy-hole states, a pseudospin operator $\vec{\tilde{j}}$ can be used to take into account a possible influence of the valence band mixing (VBM). For a VBM induced by in-plane anisotropy of the strain, the $\vec{\tilde{j}}$ components are related to the Pauli matrices $\tau$ by $\tilde{j}_z = \frac{3}{2}\tau_z$ and $\tilde{j}_\pm = \xi\tau_\pm$ with $\xi = -2\sqrt{3}\rho_s/\Delta_{\text{lh}}\exp(-2i\theta_s)$. $\rho_s$ is the coupling energy between heavy holes and light holes split by the energy $\Delta_{\text{lh}}$, and $\theta_s$ is the angle relative to the (100) axis describing the anisotropy responsible for the VBM [19].

Neglecting the VBM ($\rho_s/\Delta_{\text{lh}} \approx 0$), the 12 eigenstates of $\mathcal{H}_{h\text{-}Cr^+}$ are organized as six equally spaced doublets with defined $S_z$ and $J_z$. For each level of X$^+$-Cr$^+$ with either $M = 2$ or $M = 3$ there are six possible final states after annihilation of an electron-hole pair. With $3I_{eCr^+}$ larger than the width of the emission lines (around 75 $\mu$eV) we would expect 12 spectrally resolved PL lines for X$^+$-Cr$^+$. For a low value of $I_{eCr^+}$ (lower than a few $\mu$eV) and with $E \ll D_0$, $S_z$ is a good quantum number in the excited state (i.e., electron-Cr$^+$ states), it is conserved during the optical transition and only six lines are obtained, as observed for QD1.

For most of the QDs, the third line is split and an energy gap is observed in the center of the X$^+$-Cr$^+$ PL spectra (QD2 in Fig. 2) [19]. This structure results from (i) the presence of a VBM induced by an in-plane anisotropy which couples two by two the hole-Cr$^+$ levels and (ii) a weak electron-Cr$^+$ exchange interaction.

Provided that $\rho_s/\Delta_{\text{lh}} \ll 1$, the effect of the VBM is small on the degeneracy of all the hole-Cr$^+$ doublets except for the fourth which is split [see Fig. 3(a)]. The split states are the bonding and antibonding combinations of $|S_z = -1/2, J_z = +3/2\rangle$ and $|S_z = +1/2, J_z = -3/2\rangle$. For $3I_{eCr^+}$ larger than the width of the PL lines the optical transition to these mixed states would give rise to linearly polarized lines [9]. For a low value of $I_{eCr^+}$, the two linearly polarized transitions are degenerated, only seven lines are expected (see QD2), and the width of the central gap is controlled by $\rho_s/\Delta_{\text{lh}}$.

The distribution of PL intensity under magnetic field is opposite the situation of a Mn$^{2+}$ ion in similar CdTe/ZnTe QDs. In these dots, the level structure is dominated by an antiferromagnetic hole-Mn$^{2+}$ exchange interaction [3]. To reproduce the magnetic field dependence of the intensity distribution of X$^+$-Cr$^+$ a ferromagnetic hole-Cr$^+$ exchange interaction and a thermalization on the electron-Cr$^+$ states (i.e., initial states) with an effective temperature $T_{\text{eff}}$ are used. Based on the perturbation approach presented in Ref. [15], a ferromagnetic coupling is indeed expected for a $3d^5$ element with the hybridized triplet states (star in Fig. 1) situated above the edge of the valence band (see Supplemental Material [19]). A value of $I_{eCr^+}$ lower than a few $\mu$eV is also required to obtain the structure of six (or seven) lines. For $|I_{hCr^+}| \gg |I_{eCr^+}| \approx 0$,

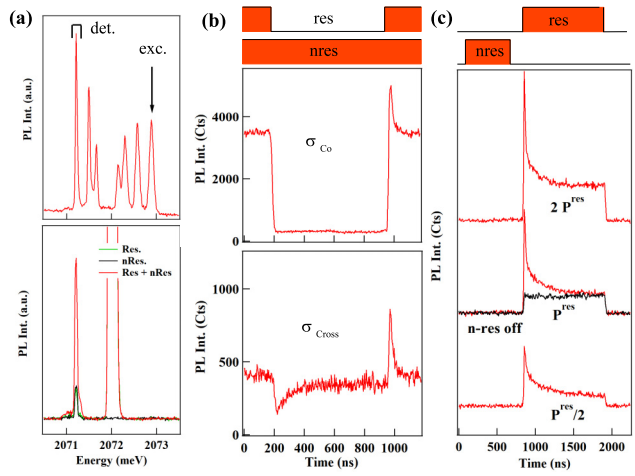


FIG. 4. (a) Configuration of excitation/detection for pumping experiments (top) and resonant PL observed on the low energy line for an excitation on the hight energy line (bottom). (b) Time resolved resonant PL obtained under continuous nonresonant (568 nm) and pulsed resonant excitations at $B = 0$ T. (c) Evolution of the pumping transients as a function of the resonant excitation power in a two pulses experiment with co-circular excitation/detection.

the hole-$Cr^+$ exchange interaction can be directly deduced from the overall splitting of the emission spectra given by $3/2 \times 5I_{h\mathrm{Cr}^+}$.

For $I_{e\mathrm{Cr}^+}$ lower than $D_0$ and $E$, the energy levels of the $X^+$-$Cr^+$ are controlled by $\mathcal{H}_{\mathrm{Cr}^+}$. In the weak magnetic field region where $g_{\mathrm{Cr}^+}\mu_B B \leqslant 6D_0$, overlaps of the different $X^+$-$Cr^+$ spin levels are possible. These states can be mixed by the $E$ term producing anticrossings in the initial state of the optical transitions. A value of $E \approx 20$ $\mu$eV is required to reproduce the spectra of QD2 below $B_z = 4$ T [Fig. 2(d) and Fig. 3(c)]. $D_0$ shifts the magnetic field position of these anticrossings. A negative $D_0$ in a few tens of $\mu$eV range has to be used to obtain most of the anticrossings in $\sigma$ polarization on the high energy side of the spectra. Depending on relative values of $D_0$ and $E$, splitting of the lines can also be observed at zero magnetic field in some of the dots [19].

With a ferromagnetic coupling, at low $T$ the hole-$Cr^+$ is in the ground states with parallel spins configuration and total angular momentum $M_z = \pm 4$. This configuration blocks the optical recombination of the excess $3d$ electron that would return the Cr atom to its $Cr^{2+}$ ground state. In analogy with dark excitons, this transition is indeed forbidden for parallel hole and $3d$ electrons spins (i.e., parallel hole and $Cr^+$ spin). The confined hole-$Cr^+$ complex is a particularly favorable system to stabilize the $Cr^+$ as the Coulomb attraction of the hole by the negative charge of the atom enhances their overlap and exchange interaction.

The two ground hole-$Cr^+$ states $M_z = \pm 4$ are not sensitive to VBM that could induce spin flip flops as observed in the case of hole-$Mn^{2+}$ [11]. This should enhance the spin memory of the hole-$Cr^+$ nanomagnet. The spin dynamics of hole-$Cr^+$ has been investigated by resonant optical pumping. For a cross-linear excitation and detection, a resonant excitation of the high energy side of $X^+$-$Cr^+$ produces only a weak resonant PL on the low energy line [Fig. 4(a)]. The resonant PL can be significantly enhanced when an additional nonresonant laser tuned below the ZnTe barrier, on the QD's excited states range, is added. The nonresonant laser produces a weak PL but has a strong influence on the intensity of the resonant fluorescence [Fig. 4(a)].

This behavior can be explained by the presence of a resonant optical pumping of the hole-$Cr^+$ spin which is partially suppressed by the nonresonant excitation. When the nonresonant excitation is combined with a pulsed resonant excitation on the high energy line, optical pumping transients are observed [Fig. 4(b)]. The resonant PL is mainly co-circularly polarized with the excitation and a transient is obtained in the emission of the low energy line. In Fig. 4(b) the resonant fluorescence obtained for co-circular excitation/detection is compared with the weaker cross-circular signal. In cross-circular configuration, the optical pumping transient is also observed in the resonant fluorescence of the low energy line. In addition, a transient is observed in the nonresonant signal just after the end of the resonant pulse. This is the direct observation in the time domain of the destruction of the pumping by the nonresonant excitation.

Under nonresonant excitation high energy phonons are generated which can contribute to a direct heating of the Cr spin [39]. $X^+$-$Cr^+$ is also formed independently of the hole-$Cr^+$ spin state. Within this complex the $Cr^+$ states are coupled by $E$ (eventually by $I_{e\mathrm{Cr}^+}$) and spin flips can occur. Both mechanisms destroy the pumping and the resonant PL is partially restored. The spin dynamics within $X^+Cr^+$ is also at the origin of the optical pumping under spin selective excitation. The larger co-polarized resonant PL suggests that spin flips of the $Cr^+$ are faster than spin flips of the electron.

When the nonresonant and resonant excitations are both modulated and separated in the time domain, an optical pumping is observed in the resonant fluorescence in co-circular excitation/detection configuration [Fig. 4(c)]. The PL intensity during the resonant pulse reaches a weak intensity plateau after a large transient. The transient is suppressed when the nonresonant excitation is switched off. Its amplitude is much larger than in the presence of the continuous nonresonant excitation showing the increase of the efficiency of the pumping. The dynamics of the optical pumping depends on the power of the resonant laser and can take place in a few tens of ns at high power. It is controlled by the probability of presence of $X^+$ and by the spin dynamics within the $X^+$-$Cr^+$ complex.

To measure the hole-$Cr^+$ spin relaxation we use a two-wavelength time resolved pumping experiment (Fig. 5). A nonresonant pulse (pulse 1) is used to initially populate the different hole-$Cr^+$ spin states. A second circularly polarized resonant pulse (pulse 2), tuned to the high-energy line of the QD, is used to perform the optical pumping (i.e., empty the hole-$Cr^+$ spin state under excitation). We use the co-circular excitation/detection configuration where the largest resonant fluorescence signal is obtained. In this configuration, the transient reflects the decrease of the absorption of the QD during the pumping process.

The hole-$Cr^+$ relaxation is probed with a third resonant pulse (pulse 3) with the same energy and polarization as pulse 2 sent after a variable dark time $\tau_d$. The amplitude of the transient during pulse 3 ($\Delta I_1$) depends on how the low-energy hole-$Cr^+$ spin state has been populated during $\tau_d$.

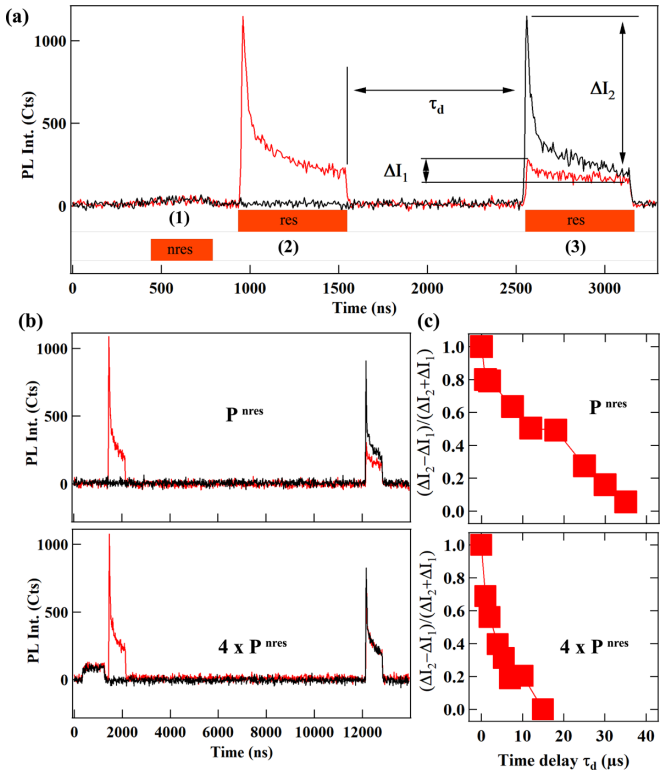


FIG. 5. (a) Three pulses resonant optical pumping experiment at $B = 0$ T in co-circular excitation/detection configuration. (b) Hole-$Cr^+$ spin relaxation observed for a fixed $\tau_d$ and two nonresonant excitation powers $P^{nres}$ and $4 \times P^{nres}$. (c) Corresponding measurements of the relaxation time.

Alternatively, pulse 2 can be suppressed and the amplitude of the pumping signal obtained during pulse 3 ($\Delta I_2$) used as a reference signal (i.e., transient in the absence of initial pumping by pulse 2).

The measured spin relaxation time is presented in Figs. 5(b) and 5(c). The dependence on $\tau_d$ of the normalized amplitude of transients $(\Delta I_2\text{-}\Delta I_1)/(\Delta I_2 + \Delta I_1)$ is shown for two values of the intensity of pulse 1. At low nonresonant excitation power a relaxation time around 20 $\mu$s can be deduced from the time evolution of the pumping transients. The relaxation time decreases with the increase of the power of the nonresonant pulse 1. As recently observed for $Cr^{2+}$, this dependence is likely to be due to the effect of phonons optically generated by the high energy excitation that remain in the sample after the end of the pulse [39].

The spin relaxation of the hole-$Cr^+$ is more than one order of magnitude longer than what was reported for the hole-$Mn^{2+}$ complex where VBM efficiently couples the spin levels [11]. VBM is still present in the case of hole-$Cr^+$ but in the ground states (i.e., $M_z = \pm 4$ with parallel hole and Cr spins), the ferromagnetic coupling of the hole and $Cr^+$ spin block the hole-$Cr^+$ flip flops. The hole-$Cr^+$ spin lifetime is then limited by the spin-lattice coupling that cannot be suppressed.

To conclude, we studied a nanomagnet based on a $Cr^+$-doped II-VI semiconductor QD. We demonstrated that the excited state of the Cr, the $Cr^+$ ionized acceptor, can be stable when inserted in a QD and exchanged coupled with a confined heavy-hole spin. The $Cr^+$ spin, not studied until now, is characterized by a ferromagnetic coupling with the hole spin and a vanishingly small exchange interaction with the electron spin. This contrast with $Cr^{2+}$ where an antiferromagnetic exchange interaction with the hole spin was observed [30,40]. The two hole-$Cr^+$ ground states with angular momentum $M_z = \pm 4$ are not sensitive to flip flops induced by VBM. The measured spin memory at $T = 4.2$ K and zero magnetic field is in the 20 $\mu$s range. It is limited by the interaction with phonons and could be further improved at sub-Kelvin temperature and weak optical excitation. The presence of $Cr^+$ could be controlled by intentional modulation doping and the hole-$Cr^+$ nanomagnet used as an efficient spin filter in transport devices operating at zero magnetic field and in the 1–2 K range.

The work was supported by the French ANR project MechaSpin (Grant No. ANR-17-CE24-0024). V.T. acknowledges support from EU Marie Curie Grant No. 754303. BigDFT calculations were done using the French supercomputers GENCI through project 6107. Work in Tsukuba was supported by the Grants-in-Aid for Challenging Exploratory Research (20K21116), Fostering Joint International Research (20KK0113), and JSPS Bilateral Joint Research Project (20219904).

[1] J. C. Oberg, M. Reyes Calvo, F. Delgado, M. Moro-Lagares, D. Serrate, D. Jacob, J. Fernandez-Rossier, and C. F. Hirjibehedin, Nature Nano. **9**, 64 (2014) and references therein.

[2] L. Bogani and W. Wernsdorfer, Nat. Mater. **7**, 179 (2008) and references therein.

[3] L. Besombes, Y. Leger, L. Maingault, D. Ferrand, H. Mariette, and J. Cibert, Phys. Rev. Lett. **93**, 207403 (2004).

[4] A. Kudelski, A. Lemaitre, A. Miard, P. Voisin, T. C. M. Graham, R. J. Warburton, and O. Krebs, Phys. Rev. Lett. **99**, 247209 (2007).

[5] O. Krebs, E. Benjamin, and A. Lemaitre, Phys. Rev. B **80**, 165315 (2009).

[6] J. Kobak, T. Smolenski, M. Goryca, M. Papaj, K. Gietka, A. Bogucki, M. Koperski, J.-G. Rousset, J. Suffczynski, E. Janik, M. Nawrocki, A. Golnik, P. Kossacki, and W. Pacuski, Nature Com. **5**, 3191 (2014).

[7] L. Besombes, C. L. Cao, S. Jamet, H. Boukari, and J. Fernandez-Rossier, Phys. Rev. B **86**, 165306 (2012).

[8] O. Krebs and A. Lemaitre, Phys. Rev. Lett. **111**, 187401 (2013).

[9] B. Varghese, H. Boukari, and L. Besombes, Phys. Rev. B **90**, 115307 (2014).

[10] R. Fainblat, C. J. Barrows, E. Hopmann, S. Siebeneicher, V. A. Vlaskin, D. R. Gamelin, and G. Bacher, Nano Lett. **16**, 6371 (2016).

[11] A. Lafuente-Sampietro, H. Boukari, and L. Besombes, Phys. Rev. B **95**, 245308 (2017).

[12] S. Lorenz, C. S. Erickson, M. Riesner, D. R. Gamelin, R. Fainblat, and G. Bacher, Nano Lett. **20**, 1896 (2020).

[13] E. V. Shornikova, D. R. Yakovlev, D. O. Tolmachev, V. Y. Ivanov, I. V. Kalitukha, V. F. Sapega, D. Kudlacik, Y. G. Kusrayev, A. A. Golovatenko, S. Shendre, S. Delikanli, H. Volkan Demir, and M. Bayer, ACS Nano **14**, 9032 (2020).
[14] J. K. Furdyna, J. Appl. Phys. **64**, R29 (1988).
[15] P. Kacman, Semicond. Sci. Technol. **16**, R25 (2001).
[16] J. Kossut and W. Dobrowolski, *Handbook of Magnetic Materials*, edited by K. H. J. Buschow (Elsevier Science Publisher, 1993), Vol. 7, Chap. 4.
[17] R. Beaulac and D. Gamelin, Phys. Rev. B **82**, 224401 (2010).
[18] P. Wojnar, C. Bougerol, E. Bellet-Amalric, L. Besombes, H. Mariette, and H. Boukari, J. Cryst. Growth **335**, 28 (2011).
[19] See Supplemental Material at http://link.aps.org/supplemental/10.1103/PhysRevB.104.L041301 for a presentation of DFT calculations techniques, a discussion on the charge states of Cr in CdTe, a discussion on the spin properties of $Cr^+$ in CdTe, a description of valence band mixing in $Cr^+$-doped QDs and additional examples of $Cr^+$-doped QDs, which includes Refs. [20–22].
[20] F. Oba, A. Togo, I. Tanaka, J. Paier, and G. Kresse, Phys. Rev. B **77**, 245202 (2008).
[21] J. P. Perdew, Int. J. Quantum Chem. **28**, 497 (1985).
[22] A. Alkauskas, P. Broqvist, and A. Pasquarello, Phys. Rev. Lett. **101**, 046405 (2008).
[23] M. Z. Cieplak, M. Godlewski, and J. M. Baranowski, Phys. Stat. Sol (b) **70**, 323 (1975).
[24] M. Godlewski and J. M. Baranowski, Phys. Stat. Sol (b) **97**, 281 (1980).
[25] L. Besombes, H. Boukari, V. Tiwari, A. Lafuente-Sampietro, M. Sunaga, K. Makita, and S. Kuroda, Phys. Rev. B **99**, 035309 (2019).
[26] L. Genovese, A. Neelov, S. Goedecker, T. Deutsch, S. A. Ghasemi, A. Willand, D. Caliste, O. Zilberberg, M. Rayson, A. Bergman, and R. Schneider, J. Chem. Phys. **129**, 014109 (2008)
[27] S. Mohr, L. E. Ratcliff, L. Genovese, D. Caliste, P. Boulanger, S. Goedecker, and T. Deutsch, Phys. Chem. Chem. Phys. **17**, 31360 (2015)
[28] C. Hartwigsen, S. Goedecker, and J. Hutter, Phys. Rev. B **58**, 3641 (1998).
[29] F. D'Acapito, P. Pochet, F. Somma, P. Aloe, R. M. Montereali, M. A. Vincenti, and S. Polosan, Appl. Phys. Lett. **102**, 081107 (2013).
[30] A. Lafuente-Sampietro, H. Utsumi, M. Sunaga, K. Makita, H. Boukari, S. Kuroda, and L. Besombes, Phys. Rev. B **97**, 155301 (2018).
[31] The intensity of the third line is weaker showing that it starts to be split.
[32] Y. Léger, L. Besombes, L. Maingault, and H. Mariette, Phys. Rev. B **76**, 045331 (2007).
[33] Different from the negatively charged acceptor $Mn^{2+}$ in III-V semiconductor compounds where a strong localization of the hole is observed [4,34,35]. This probably arises from a lager extension of the electron wave function on the negatively charged $Cr^+$ (acceptor close to the conduction band) and consequently to a weaker central cell correction to the Coulomb potential.
[34] A. K. Bhattacharjee and C. Benoit à la Guillaume, Solid State Comm **113**, 17 (2000).
[35] T. Dietl, F. Matsukura, and H. Ohno, Phys. Rev. B **66**, 033203 (2002).
[36] G. W. Ludwig and M. R. Lorenz, Phys. Rev. **131**, 601 (1963).
[37] A. H. Trojnar, M. Korkusinski, U. C. Mendes, M. Goryca, M. Koperski, T. Smolenski, P. Kossacki, P. Wojnar, and P. Hawrylak, Phys. Rev. B **87**, 205311 (2013).
[38] A. Lafuente-Sampietro, H. Boukari, and L. Besombes, Phys. Rev. B **92**, 081305(R) (2015).
[39] V. Tiwari, K. Makita, M. Arino, M. Morita, S. Kuroda, H. Boukari, and L. Besombes, Phys. Rev. B **101**, 035305 (2020).
[40] L. Besombes, H. Boukari, V. Tiwari, A. Lafuente-Sampietro, S. Kuroda, and K. Makita, Semicond. Sci. Technol. **34**, 063001 (2019).